Japanese Journal of Radiology
https://doi.org/10.1007/s11604-024-01635-y

REVIEW

Review of whole-body magnetic resonance imaging in multiple myeloma

Teresa Perillo[1] · Claudia Giorgio[2] · Arianna Fico[2] · Marianna Perrotta[1] · Antonietta Serino[1] · Renato Cuocolo[2] · Andrea Manto[1]

Received: 19 February 2024 / Accepted: 22 July 2024

Abstract
Multiple Myeloma (MM) is a hematological malignancy affecting bone marrow, most frequently in elderly men. Imaging has a crucial role in this disease. Recently, whole-body MRI has been introduced and it has gained growing interest due to is high sensitivity and specificity in evaluating bone marrow involvement in MM. Diffusion-weighted sequences (DWI) with apparent diffusion coefficient (ADC) maps have emerged as the most sensitive technique to evaluate patients with MM, both in the pre- and post-treatment setting. Aim of this review is to provide an overview of the role and main imaging findings of whole-body MRI in MM.

Keywords Multiple Myeloma · Whole-body magnetic resonance imaging · Oncologic imaging · Diffusion weighted imaging

Introduction

Multiple myeloma (MM) is a hematological malignancy affecting the bone marrow, characterized by monoclonal proliferation of mature plasma cells [1]. It mainly affects the elderly population, with an average age at diagnosis of 66 years [2]. MM is characterized by an overproduction of monoclonal immunoglobulins in the blood and/or urine and the presence of bone lesions [3]. It evolves from a premalignant condition called monoclonal gammopathy of undetermined significance (MGUS) and smoldering MM, which finally becomes symptomatic MM [4]. MM begins with monoclonal expansion of malignant cells in the bone marrow which interact with stromal cells, shifting the balance towards an excess of osteoclast activation factors and a suppression of osteoblast activity. Cytokines produced by stromal cells lead to proliferation of MM clones, thus generating a vicious cycle, as bone destruction fuel monoclonal cell growth [5].

Magnetic Resonance Imaging (MRI) is the gold standard in MM due to its excellent soft-tissue contrast, which allows bone marrow evaluation with high sensitivity [6]. The introduction of diffusion-weighted imaging (DWI) has improved the application of MRI in MM as it enables cellular density evaluation [7]. Furthermore, different studies have shown that there is a direct relationship between apparent diffusion coefficient (ADC) values and cell density, which enables accurate response assessment [8–10]. Therefore, DWI with ADC maps have been included in the MRI protocol for MM, which is called WB-MRI, and has emerged as the most sensitive technique for bone marrow imaging in MM [11].

Aim of this review is to provide an overview of the current imaging guidelines in MM, with a focus on the main imaging findings of WB-MRI in MM.

Imaging in MM

The International Myeloma Working Group (IMWG) has defined diagnostic criteria for MM, which include clonal plasma cells of bone marrow greater than 10% or biopsy-proven bone or extramedullary plasmacytoma and one or more of the following myeloma defining events [12, 13]:

✉ Teresa Perillo
tperillo3@gmail.com

[1] Neuroradiology Unit, Umberto I" Hospital, Nocera Inferiore, Italy

[2] Department of Medicine, Surgery, and Dentistry, University of Salerno, Fisciano, Italy

Published online: 01 August 2024

- Evidence of end-organ damage, guided by CRAB criteria (Calcium elevation, Renal insufficiency, Anemia, and Bone disease): serum calcium > 11,5 mg/ dl; kidney failure; serum creatinine > 2.0 mg/dl; anemia: Hemoglobin level < 10 mg/dl; presence of lytic bone lesions.
- One or more of the following biomarkers of malignancy: medullary monoclonal plasma cells of 60% or more; serum free light chain ratio (Involved Chain/Uninvolved Chain) greater than 100; at least one focal lesion in MRI studies greater than 5 mm.

Imaging in MM is used to establish bone involvement, which is necessary for risk stratification, patient management and detection of residual disease after treatment (Figs. 1 and 2) [14].

IMWG has also defined bone involvement in MM as follows [15]:

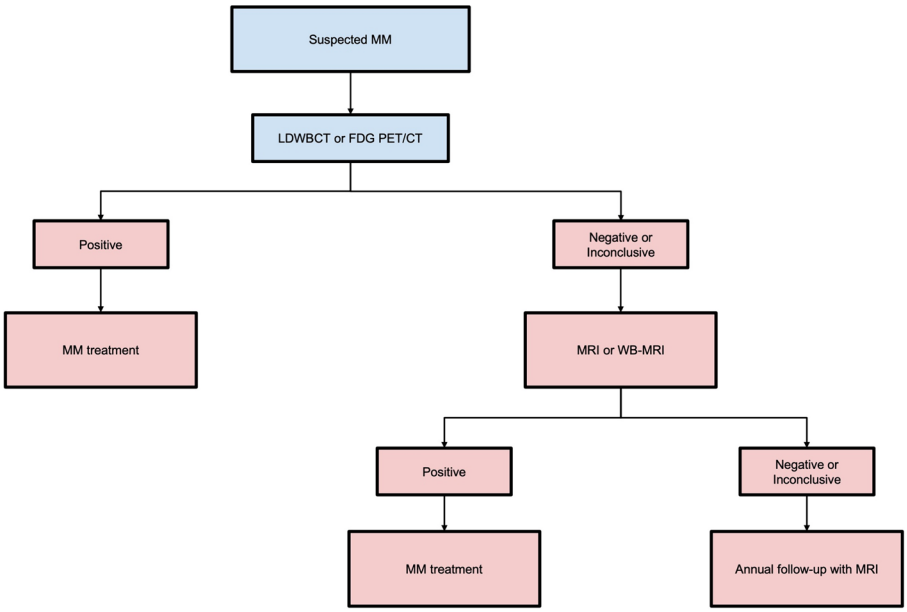

Fig. 1 Algorithm summarizing recommendations for imaging techniques in suspected MM. *MM* Multiple Myeloma, *LDWBCT* low-dose whole body CT, *FDG PET/CT* fluorodeoxyglucose positron emission tomography/computed tomography

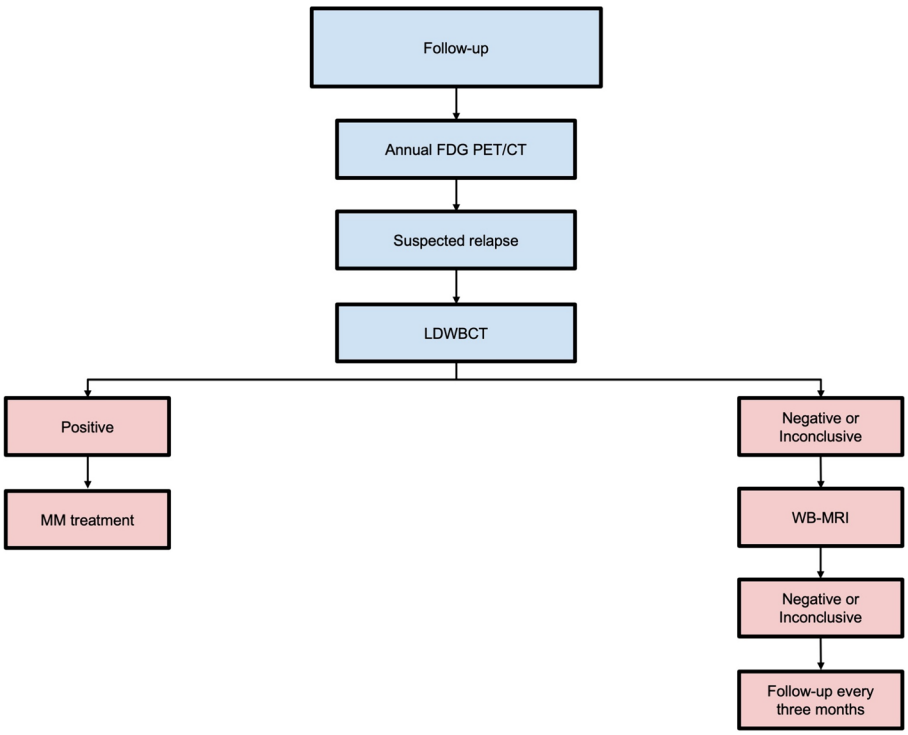

Fig. 2 Algorithm summarizing recommendations for imaging techniques in suspected follow-up. *MM* Multiple Myeloma, *LDWBCT* low-dose whole body CT, *FDG PET/CT* fluorodeoxyglucose positron emission tomography/computed tomography

- CT: one or more osteolytic lesions (diameter ≥ 5 mm).
- [^{18}F]FDG-positron emission tomography (PET)/CT: one or more osteolytic lesions (diameter ≥ 5 mm). Increased [^{18}F]FDG uptake alone is not sufficient; evidence of osteolytic bone destruction is required on CT.
- MRI or WB-MRI: > 1 focal lesion with a diameter ≥ 5 mm. Diffuse marrow abnormality does not qualify.

Conventional skeletal radiographic investigation has been used for decades to assess bone disease in MM [16]. However, it can only detect advanced stages of MM, which are characterized by lytic lesions without surrounding reactive sclerosis. Furthermore, conventional skeletal radiographic cannot distinguish osteopenia caused by MM from the other more common causes of this condition, such as osteoporosis and steroid use [17]. Therefore, international guidelines recommend the use of more advanced imaging techniques, such as low-dose whole-body CT (LDWBCT), [^{18}F]FDG-PET/CT and WB-MRI [18].

LDWBCT is useful for detection of osteolytic lesions in MM, but it cannot evaluate early bone marrow infiltration [16]. Moreover, LDWBCT cannot discriminate between active and treated lesions [15].

[^{18}F]FDG—PET/CT adds quantitative information on glucose metabolism, providing a combination of anatomical and functional information that can be used to assess the extent of bone marrow disease (both skeletal and extramedullary) and the response to therapy [5]. [^{18}F]FDG-PET/CT can distinguish between metabolically active and inactive lesions, allowing the evaluation of treatment efficacy [19]. Limitations of [^{18}F]FDG-PET/CT include low spatial resolution, use of radiation and inability to detect bone marrow lesions [11].

WB-MRI has shown high sensitivity and specificity for early detection of bone marrow infiltration by monoclonal cells (with sensitivity and specificity of 89% and 87%, respectively) [20]. In particular, WB-MRI identifies bone marrow lesions in MM which are not detectable with [^{18}F]FDG-PET/CT and diffuse bone marrow infiltration [21]. Diffusion-weighted imaging (DWI) paired with apparent diffusion coefficient (ADC) maps have emerged as the most sensitive sequences of WB-MRI, allowing qualitative and quantitative assessment of disease as well as response to therapy [22]. In post-treatment setting, WB-MRI has shown a sensitivity of 90% and a specificity of 66% [23].

WB-MRI protocol is designed to detect MM lesions within the bone marrow, but it can also visualize extramedullary diseases and acquisition time is of about 45 min [24]. The protocol consists of [7]:

- sagittal whole spine T1-weighted, T2-weighted and STIR (or fat suppressed T2-weighted) sequences, section thickness of 4-5 mm;
- axial whole body (skull vertex to knees) DWI (b-values: 50–100 s/mm^2 and 800–900 s/mm^2),5 mm thickness with corresponding ADC map and 3D maximum intensity projection reconstruction;
- axial whole body (skull vertex to knees) T1-weighted Dixon sequence with 5 mm thickness.

Axial T2-weighted whole-Body (vertex to knees) images are optional [5]. For patients with symptoms, sagittal spine imaging should be performed first to detect mechanical complications (such as vertebral fractures or expansive disease compressing the spinal cord or nerve roots) in case of premature scanning interruption [5].

WB-MRI findings

Normal MRI findings

Normal bone marrow is composed of red (or hematopoietic) marrow, yellow (or fatty) marrow and trabecular bone in varying proportions, depending on the age of the patient [25]. At birth, the entire bone marrow is metabolically active, but gradually, with growth, it turns into a metabolically less active marrow. MRI bone signal depends on the proportion of red and yellow marrow [26]. MRI is the imaging modality of choice to monitor bone marrow changes due to its rich soft tissue contrast [27]. Normal yellow bone marrow signal on MRI is hyperintense on T1-weighted images, hyperintense on T2-weighted sequences, and it appears hypointense than muscles on STIR images (Fig. 3) [28]. Red bone marrow shows low to intermediate signal intensity compared to intervertebral discs on T1-weighted images, and intermediate signal intensity on T2-weighted and STIR sequences [28]. With increasing age, red bone marrow evolves into yellow bone marrow in a process called "conversion", resulting in a prevalence of fat [29].

DWI

In MM, MRI may be normal or show different patterns of bone marrow involvement such as focal, diffuse (Fig. 4) or micronodular. Concurrent pathologic fractures that mimic a benign pattern may be present [28].

In the past few years, the evaluation of the bone marrow with DWI and ADC maps has gained a central role [30]. DWI is a highly sensitive functional imaging technique that produces images where contrast between tissues is based on differences in the motion of water molecules at a cellular level, thus it enables evaluation of cell density [31]. In particular, the greater the cellularity of a tissue (such as tumor tissue), the smaller will be the movement of water molecules. This will translate into an increase of signal DWI

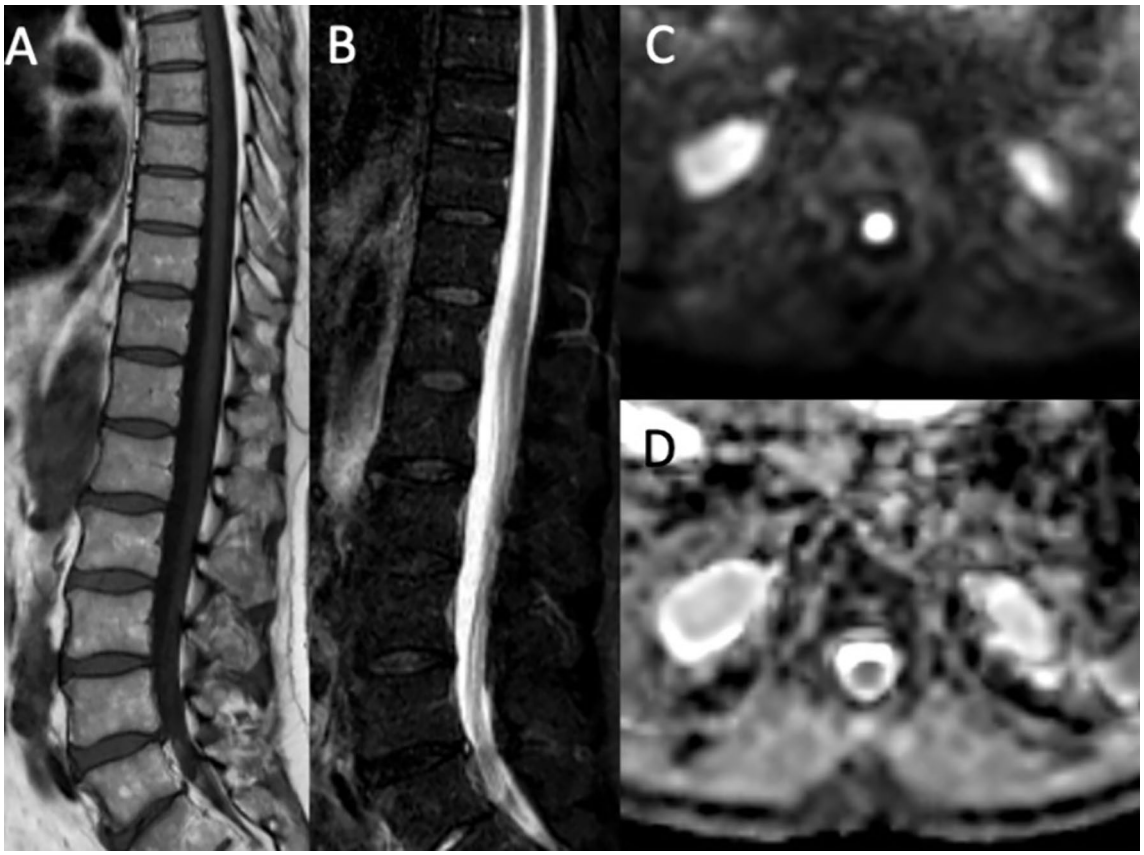

Fig. 3 Normal bone marrow in a 19-year-old woman. Normal bone marrow in a 19-year-old woman appears hyperintense on sagittal T1-weighted image (**A**), hypointense on sagittal STIR (**B**), and hypointense on DWI (**C**). ADC value is 400×10^{-6} mm2 s.$^{-1}$ on ADC map (**D**)

sequences (compared to the surrounding background) and a reduction in ADC values that represents quantitative value of this movement. Therefore, ADC values are inversely proportional to cellularity: the more cells there are, the less water movements and thus lower ADC [32]. ADC values of normal bone marrow are less than 600×10^{-6} mm^2 s^{-1}, with even lower values in elderly patients, where fat marrow prevails and limits water movement [33]. On the other hand, MM bone marrow lesions show ADC values between 600–700 and 1400×10^{-6} mm^2 s^{-1} (Figs. 5 and 6) whereas after treatment ADC values are higher than 1400×10^{-6} mm^2 s^{-1} due to increased interstitial water induced by cell death and vascular congestion (Fig. 7) [34].

T1 Dixon

T1-weighted sequences with Dixon technique for fat-suppression is an important sequence of WB-MRI for the evaluation of bone lesions in MM [35]. Separation of fat and water based on the "chemical shift", generates four Dixon images, which are called In-Phase (IP), Out-of-Phase (OP), Fat-Only (FO) and Water-Only (WO). The FO and WO images have proved to be useful in detection of focal lesions in MM, more significantly than IP images. Focal lesions are typically hypointense compared to background marrow on IP and FO sequences, while they appear hyperintense on the WO images (Fig. 8) [36].

Treatment response evaluation

WB-MRI is a powerful tool to evaluate response to treatment in patients with MM [37]. Early response to therapy is characterized by edema and bone marrow hemorrhage due to cell death and vascular congestion; these changes induce an increase in interstitial water, resulting in increased ADC values [38]. Treated lesions also show higher signal on T2-weighted images and lower signal on T1-weighted sequences (Fig. 9) [39]. During follow-up, treated lesions show signs of fat conversion, which determine an increased signal in T1-weighted images, decreased signal in T2-weighted sequences and a reduction of ADC values (Fig. 10) [30, 34].

Finally, fat fraction maps derived from the Dixon sequences provide data regarding treatment as in responding lesions normal fat is restored [15]. Dixon sequences show increased signal on FO and decreased signal on WO

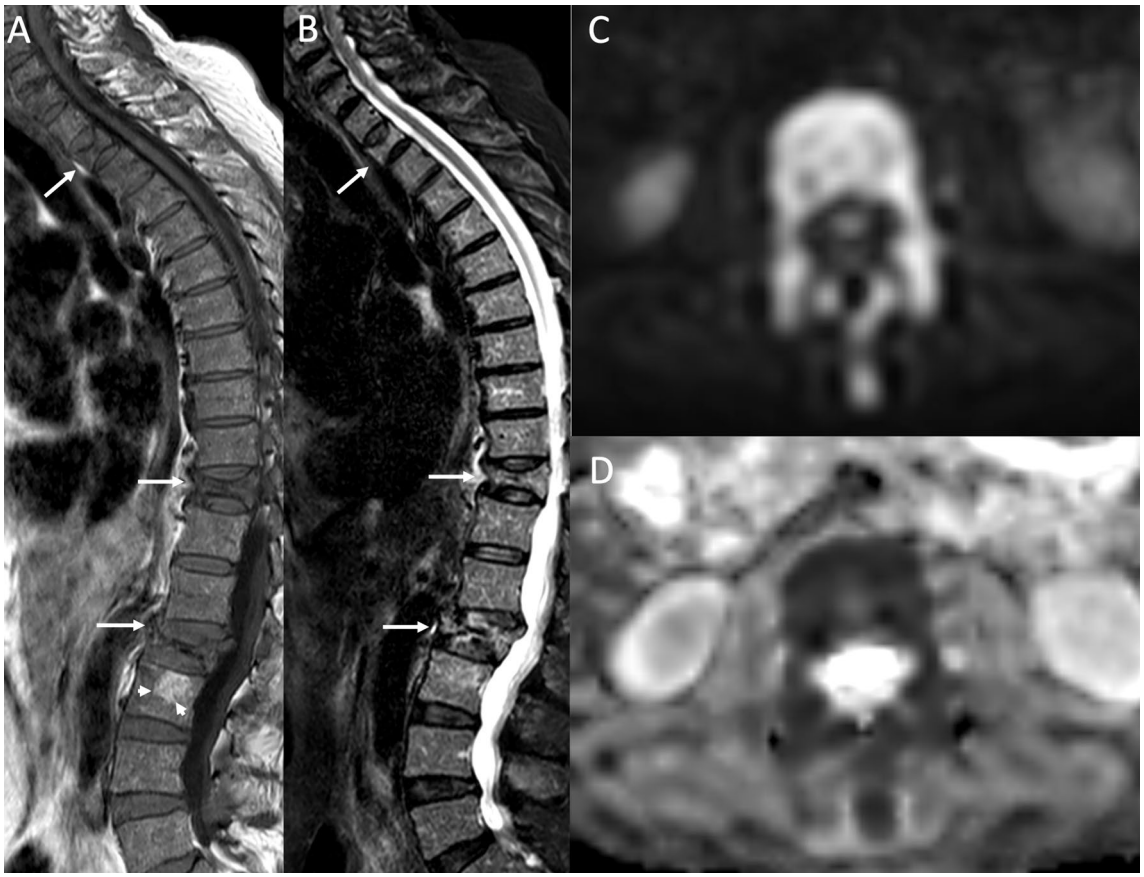

Fig. 4 Diffuse bone marrow involvement in a 78-year-old male patient with Multiple Myeloma. Bone marrow diffusely appears hypointense on T1-weighted image (**A**), hyperintense on sagittal STIR (**B**) and axial DWI (**C**). ADC value is 900×10^{-6} mm^2 s^{-1} on ADC map (**D**). Note also multiple vertebral fractures (arrows in A and B) and a vertebral hemangioma (arrowheads in **A**). The patient died 1 year later

sequences compared to pre-treatment lesions [40]. Furthermore, after treatment, T1-weighted sequences with fat-suppression with Dixon technique show an increase in the signal on FO and a decrease in the signal on WO sequences, possibly becoming an early biomarker of response to therapy [35].

Extramedullary disease

Malignant plasma cells in MM are typically confined to the bone marrow. However, extramedullary plasmacytomas may develop, with an incidence between 7 and 18% [40]. Extramedullary plasmacytomas can infiltrate in two ways. In extramedullary disease infiltration arises from hematogenous spread whereas in paramedullary disease soft tissue infiltration occurs due to direct growth from skeletal tumors following cortical bone disruption (Fig. 11) [41]. Extramedullary disease is an aggressive form of MM with poor prognosis, high mortality rate and a short overall survival time [42]. These lesions develop not only in paraspinal or epidural sites, but also in solid organs, nodes, skin and retroperitoneum [40]**.** WB-RM can be useful in assessing extramedullary and paramedullary lesions and the extent of soft tissue disease [43].

Differential diagnosis

Vertebral hemangioma is the most common benign vertebral tumor. DWI images with ADC maps, combined with appearances on T1- and T2-weighted images of the spine, should avoid misdiagnoses [44]. Vertebral hemangiomas appear as a roundish lesion hyperintense on T1 and T2-weighted images, with variable fat suppression depending on the amount of fat components (Figs. 4 and 12) [45]. In vertebral hemangioma, ADC values are significantly higher than active myeloma deposits, thus allowing distinction [46].

Bone marrow biopsy may also be a confounding factor as iliac trephine tract may cause local hematoma, which show restricted diffusion, mimicking active disease [5]. Therefore, a solitary lesion in the posterior iliac crest should be carefully interrogated for the presence of a trephine tract.

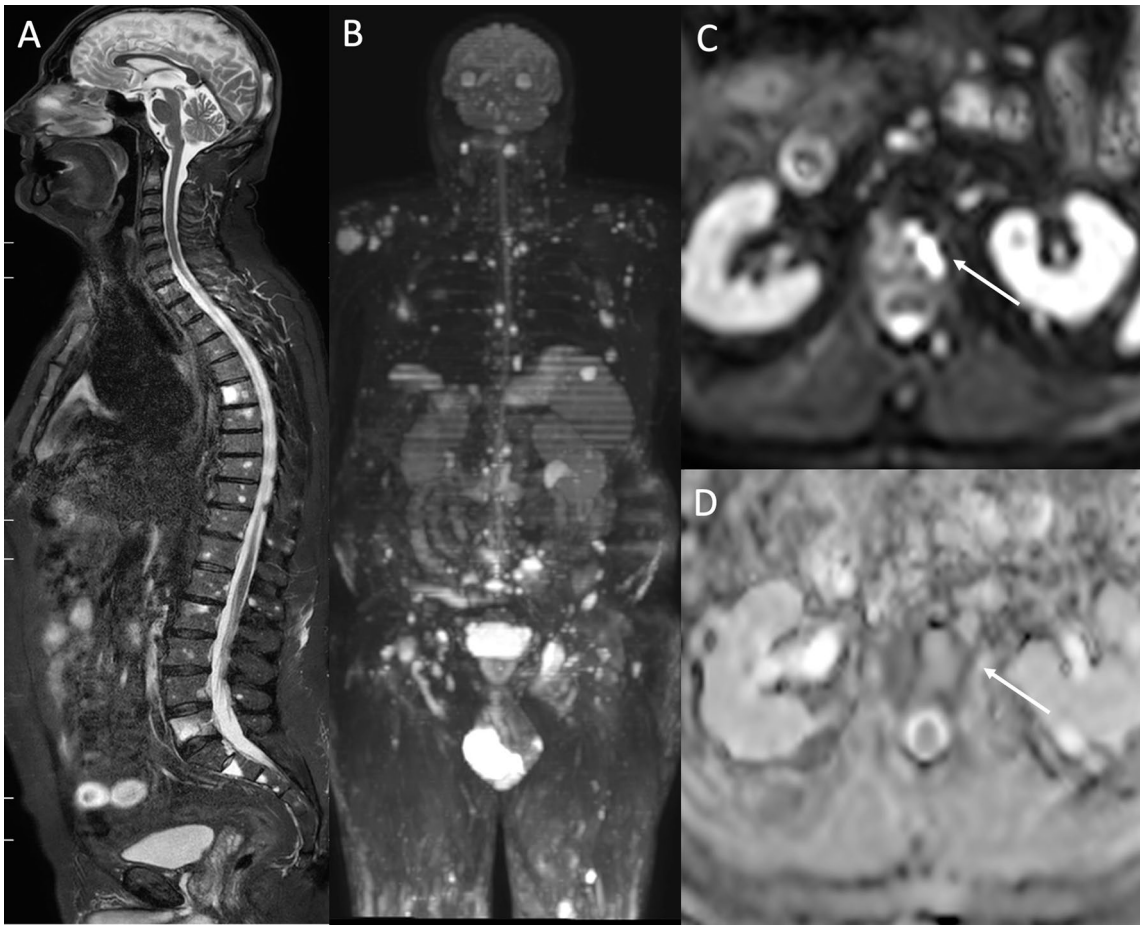

Fig. 5 Focal lesions in a 56-year-old male patient with Multiple Myeloma. Multiple focal lesions appear hyperintense on sagittal STIR (**A**) and coronal maximum intensity projection of DWI (**B**) and axial DWI (arrow **C**). ADC value is 1000×10^{-6} mm^2 s^{-1} on ADC map (**D**). The patient is doing chemotherapy and he is followed at our institution

Limitations

Although promising, WB-MRI has some limitations. Firstly, acquisition time is long, and it can be challenging for patients with MM to stay in the supine position for over 45 min, especially in case vertebral fractures. Secondly, WB-MRI has shown a sensitivity of approximately 90%, but the specificity is relatively lower, especially in the post-treatment setting (approximately of 66%) [23].

Finally, MRI is an expensive technique, which requires specific expertise, and it is still not widely available.

Future perspective

A possible solution to long acquisition time of WB-MRI could be the introduction of abbreviated protocols in selected cases [47], but their diagnostic accuracy still has to be evaluated.

On the other hand, the evaluation of fat fraction could be used to improve specificity. Fat fraction is a MRI technique which enables the production of maps whose signal results from fat protons divided by the sum of the signals from fat and water protons, thus giving information about fat content of tissues [48]. It is useful to evaluate post-treatment response of lesions in MM, as they show increased fat content [49].

Conclusion

The advent of WB-MRI has enabled accurate qualitative and quantitative assessment of disease burden in MM, especially though the use of DWI with ADC maps and Dixon T1-weighted sequences. Therefore, it is important for the radiologist to be familiar with this imaging technique.

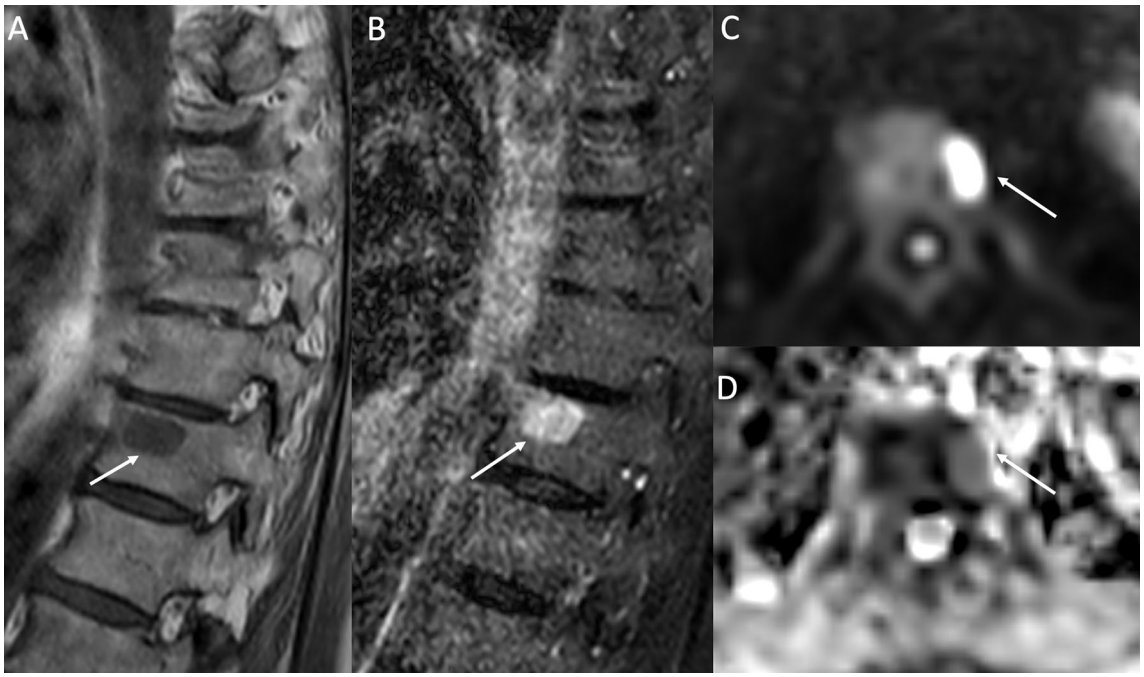

Fig. 6 Focal lesion in a 67-year-old female patient with Multiple Myeloma. Focal lesion is hypointense on sagittal T1 image (arrow in **A**) and hyperintense on sagittal STIR and axial DWI (arrow in **B** and **C**). ADC values is 1100×10^{-6} mm^2 s^{-1} on ADC map (**D**). The patient is doing chemotherapy and she is followed at our institution

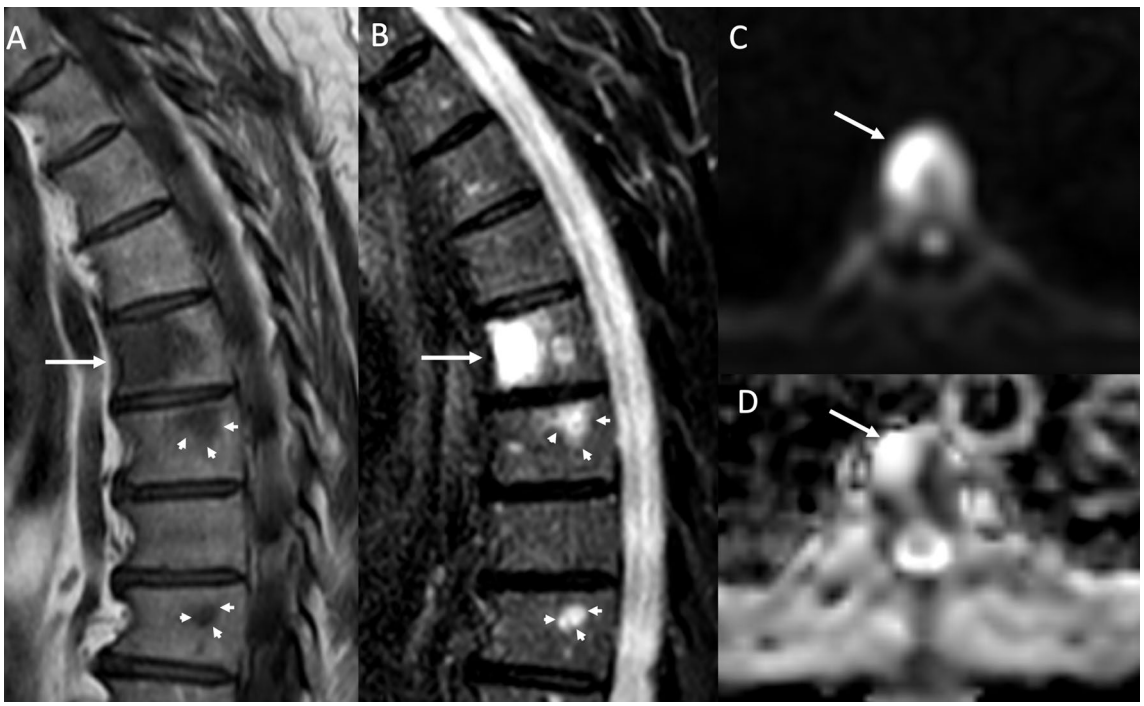

Fig. 7 Focal lesion changes after treatment in a 79-year-old male patient with Multiple Myeloma. Focal lesion appears hypointense on sagittal T1 (arrow in **A**), and hyperintense on STIR and axial DWI (arrow in **B** and **C**). ADC values is 2200×10^{-6} mm^2 s^{-1} on ADC map (**D**). Note also other focal lesions (arrowheads in **A** and **B**). The patient is doing chemotherapy and he is followed at our institution

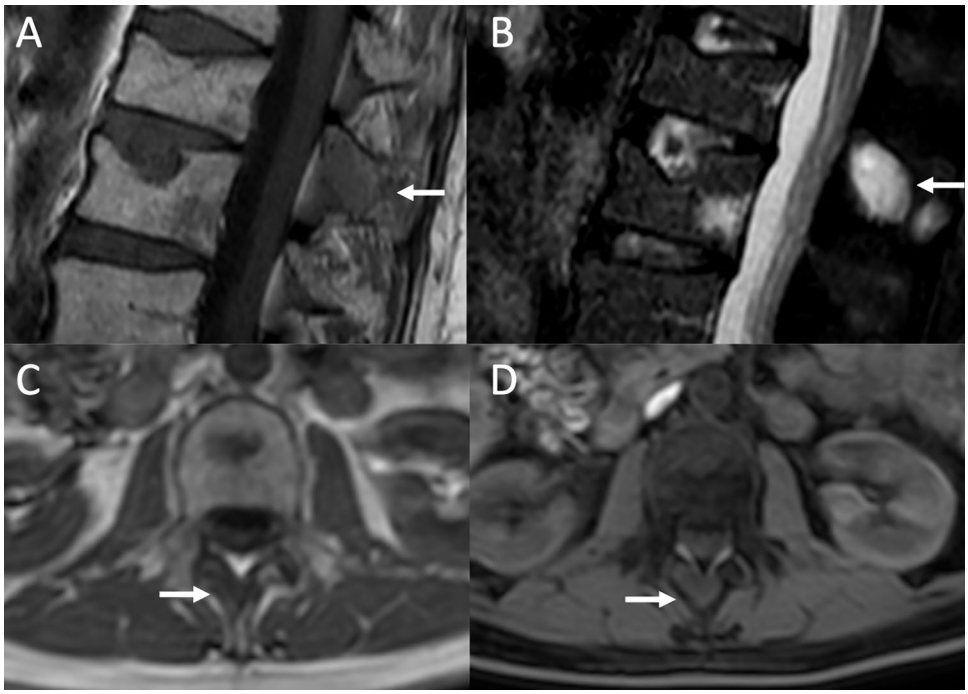

Fig. 8 Focal lesion in a 65-year-old male patient with Multiple Myeloma. Focal lesion appears hypointense on sagittal T1 (arrow in **A**), hyperintense on sagittal STIR (arrow in **B**), and it shows low signal on T1 Dixon Fat-Only (arrow in **C**) and high signal on T1 Dixon Water-Only (arrow in **D**) compared to normal bone marrow. He has a stable clinical condition and he is followed at our institution

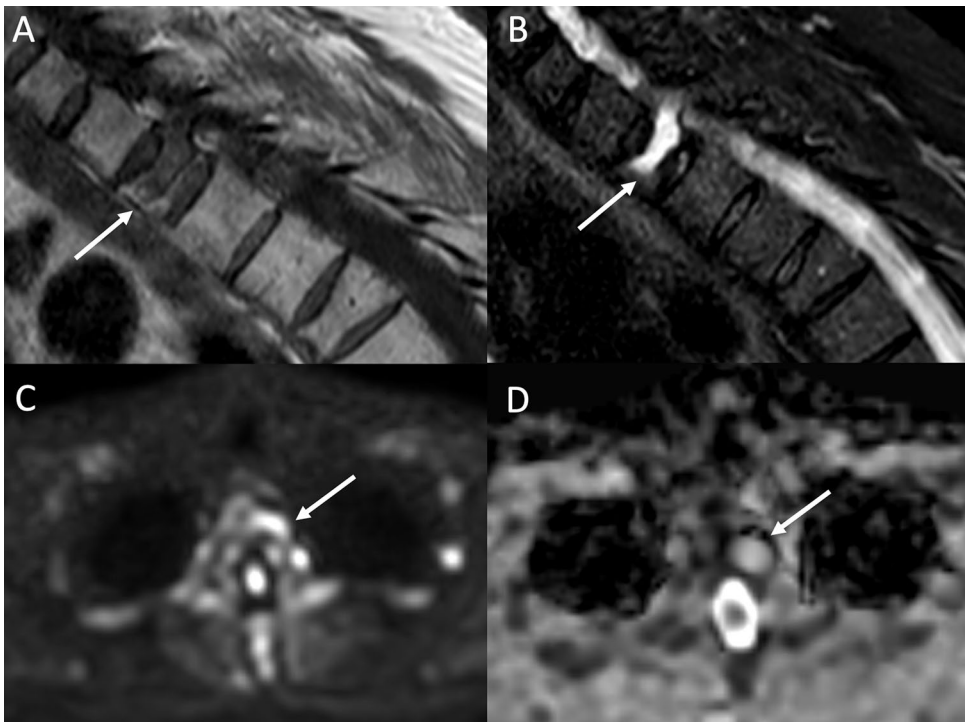

Fig. 9 Early signal alterations of a focal lesion after treatment in a 76-year-old male patient with Multiple Myeloma. Focal lesion appears hypointense on sagittal T1 image (arrow in **A**), hyperintense on sagittal STIR and axial DWI (arrow in **B** and **C**). ADC values is 2300×10^{-6} mm^2 s^{-1} on ADC map (**D**). Note also the fracture of the vertebra in A and B. He has a stable clinical condition and is followed at our institution

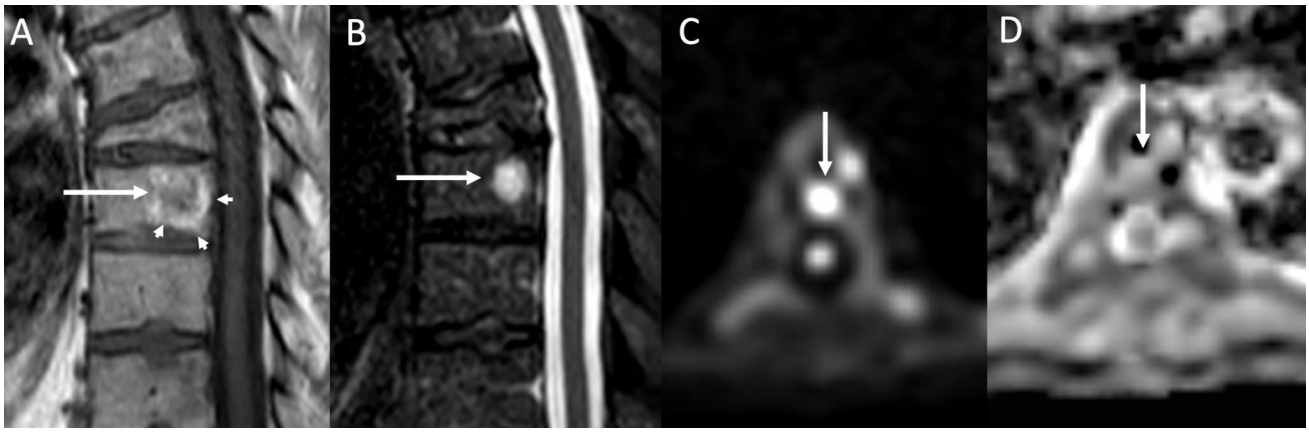

Fig. 10 Late signal alteration of a focal lesion after treatment in a 57-year-old male patient with Multiple Myeloma. Focal lesion is inhomogeneously hypointense on sagittal T1 (arrow in **A**) due to the presence of fatty tissue peripherally (arrowheads in A). On sagittal STIR (B) and axial DWI (**C**) the focal lesion is hyperintense and fat is suppressed on STIR. ADC value is 1500×10^{-6} mm^2 s^{-1} on ADC map (**D**). He has a stable clinical condition and is followed at our institution

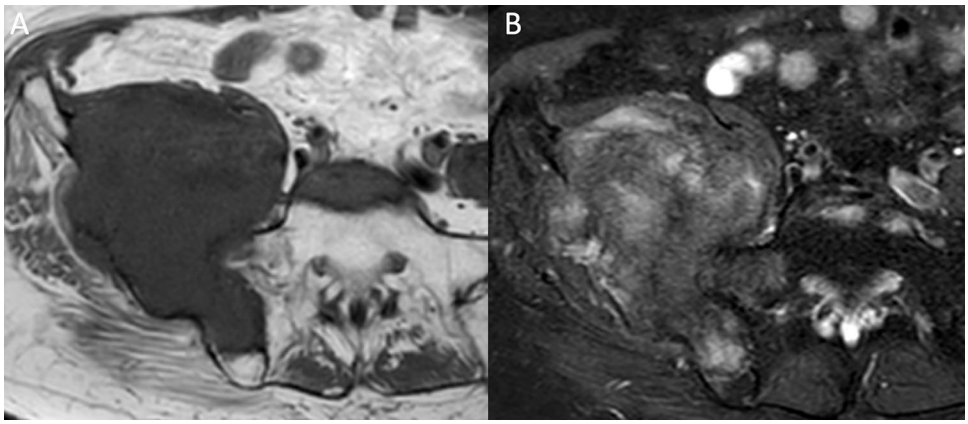

Fig. 11 Paramedullary mass in the right hip of a 66-year-old female patient with Multiple Myeloma. The voluminous mass appears inhomogeneously hypointense on axial T1 (**A**) and STIR (**B**) images. The patient died 6 months after the exam

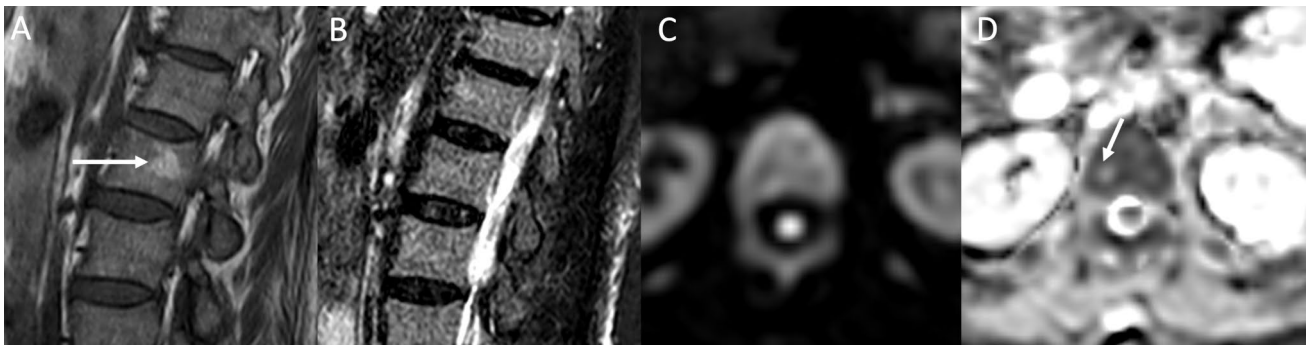

Fig. 12 Vertebral hemangioma in a 35-year-old woman. Vertebral hemangioma appears hyperintense on sagittal T1 image (**A**), isointense on STIR (**B**) and axial DWI (**C**). ADC values is 2200×10^{-6} mm^2 s.$^{-1}$ on ADC map (**D**)

Author contributions Study concepts: TP, AM. Data acquisition: MP, AS. Manuscript preparation: CG, AF. Manuscript editing: TP, RC. Manuscript review: TC, RC.

Declarations

Conflict of interest The authors have no relevant financial or non-financial interests to disclose.

Ethical approval Ethical approval not required.

Informed consent Informed consent was obtained.

Consent to participate Consent to participate was obtained.

References

1. International Myeloma Working Group. Criteria for the classification of monoclonal gammopathies, multiple myeloma and related disorders: a report of the International Myeloma Working Group. Br J Haematol. 2003;121:749–57.
2. Kyle RA, Gertz MA, Witzig TE, et al. Review of 1027 patients with newly diagnosed multiple myeloma. Mayo Clin Proc. 2003;78:21–33. https://doi.org/10.4065/78.1.21.
3. Angtuaco EJC, Fassas ABT, Walker R, et al. Multiple myeloma: clinical review and diagnostic imaging. Radiology. 2004;231:11–23. https://doi.org/10.1148/radiol.2311020452.
4. Landgren O, Kyle RA, Rajkumar SV. From myeloma precursor disease to multiple myeloma: new diagnostic concepts and opportunities for early intervention. Clin Cancer Res. 2011;17:1243–52. https://doi.org/10.1158/1078-0432.CCR-10-1822.
5. Messiou C, Kaiser M. Whole-Body Imaging in Multiple myeloma. Magn Reson Imaging Clin N Am. 2018;26:509–25. https://doi.org/10.1016/j.mric.2018.06.006.
6. Moulopoulos LA, Dimopoulos MA, Weber D, et al. Magnetic resonance imaging in the staging of solitary plasmacytoma of bone. JCO. 1993;11:1311–5. https://doi.org/10.1200/JCO.1993.11.7.1311.
7. Messiou C, Hillengass J, Delorme S, et al. Guidelines for acquisition, interpretation, and reporting of whole-body MRI in Myeloma: Myeloma Response Assessment and Diagnosis System (MY-RADS). Radiology. 2019;291:5–13. https://doi.org/10.1148/radiol.2019181949.
8. Hillengass J, Landgren O. Challenges and opportunities of novel imaging techniques in monoclonal plasma cell disorders: imaging "early myeloma." Leuk Lymphoma. 2013;54:1355–63. https://doi.org/10.3109/10428194.2012.740559.
9. Hillengass J, Bäuerle T, Bartl R, et al. Diffusion-weighted imaging for non-invasive and quantitative monitoring of bone marrow infiltration in patients with monoclonal plasma cell disease: a comparative study with histology. Br J Haematol. 2011;153:721–8. https://doi.org/10.1111/j.1365-2141.2011.08658.x.
10. Giles SL, Messiou C, Collins DJ, et al. Whole-body diffusion-weighted mr imaging for assessment of treatment response in myeloma. Radiology. 2014;271:785–94. https://doi.org/10.1148/radiol.13131529.
11. Pawlyn C, Fowkes L, Otero S, et al. Whole-body diffusion-weighted MRI: a new gold standard for assessing disease burden in patients with multiple myeloma? Leukemia. 2016;30:1446–8. https://doi.org/10.1038/leu.2015.338.
12. Kyle RA, Rajkumar SV. Criteria for diagnosis, staging, risk stratification and response assessment of multiple myeloma. Leukemia. 2009;23:3–9. https://doi.org/10.1038/leu.2008.291.
13. Rajkumar SV. Multiple myeloma: every year a new standard? Hematol Oncol. 2019;37:62–5. https://doi.org/10.1002/hon.2586.
14. Lee K, Kim KW, Ko Y, et al. Comprehensive updates in the role of imaging for multiple myeloma management based on recent International Guidelines. Korean J Radiol. 2021;22:1497. https://doi.org/10.3348/kjr.2020.0886.
15. Barwick T, Bretsztajn L, Wallitt K, et al. Imaging in myeloma with focus on advanced imaging techniques. BJR. 2019;92:20180768. https://doi.org/10.1259/bjr.20180768.
16. Ormond Filho AG, Carneiro BC, Pastore D, et al. Whole-body imaging of multiple myeloma: diagnostic criteria. Radiographics. 2019;39:1077–97. https://doi.org/10.1148/rg.2019180096.
17. Ferraro R, Agarwal A, Martin-Macintosh EL, et al. MR imaging and PET/CT in diagnosis and management of multiple myeloma. Radiographics. 2015;35:438–54. https://doi.org/10.1148/rg.352140112.
18. Guha A, Vijan A, Agarwal U, et al. Imaging for plasma cell dyscrasias: What, When, and How? Front Oncol. 2022;12: 825394. https://doi.org/10.3389/fonc.2022.825394.
19. Cavo M, Terpos E, Nanni C, et al. Role of 18F-FDG PET/CT in the diagnosis and management of multiple myeloma and other plasma cell disorders: a consensus statement by the International Myeloma Working Group. Lancet Oncol. 2017;18:e206–17. https://doi.org/10.1016/S1470-2045(17)30189-4.
20. Suh CH, Yun SJ, Jin W, et al. ADC as a useful diagnostic tool for differentiating benign and malignant vertebral bone marrow lesions and compression fractures: a systematic review and meta-analysis. Eur Radiol. 2018;28:2890–902. https://doi.org/10.1007/s00330-018-5330-5.
21. Dimopoulos M, Terpos E, Comenzo RL, et al. International myeloma working group consensus statement and guidelines regarding the current role of imaging techniques in the diagnosis and monitoring of multiple Myeloma. Leukemia. 2009;23:1545–56. https://doi.org/10.1038/leu.2009.89.
22. Sachpekidis C, Mosebach J, Freitag MT, et al. Application of (18) F-FDG PET and diffusion weighted imaging (DWI) in multiple myeloma: comparison of functional imaging modalities. Am J Nucl Med Mol Imag. 2015;5:479–92.
23. Rama S, Suh CH, Kim KW, et al. Comparative performance of whole-body MRI and FDG PET/CT in evaluation of multiple myeloma treatment response: systematic review and meta-analysis. Am J Roentgenol. 2022;218:602–13. https://doi.org/10.2214/AJR.21.26381.
24. Winfield JM, Blackledge MD, Tunariu N, et al. Whole-body MRI: a practical guide for imaging patients with malignant bone disease. Clin Radiol. 2021;76:715–27. https://doi.org/10.1016/j.crad.2021.04.001.
25. Swartz PG, Roberts CC. Radiological reasoning: bone marrow changes on MRI. Am J Roentgenol. 2009;193:S1–4. https://doi.org/10.2214/AJR.09.7069.
26. Vande Berg BC, Malghem J, Lecouvet FE, Maldague B. Magnetic resonance imaging of the normal bone marrow. Skeletal Radiol. 1998;27:471–83. https://doi.org/10.1007/s002560050423.
27. Karampinos DC, Ruschke S, Dieckmeyer M, et al. Quantitative MRI and spectroscopy of bone marrow. Magn Reson Imag. 2018;47:332–53. https://doi.org/10.1002/jmri.25769.
28. Caranci F, Tedeschi E, Ugga L, et al. Magnetic Resonance Imaging correlates of benign and malignant alterations of the spinal bone marrow. Acta Biomed 2018;89:18–33. https://doi.org/10.23750/abm.v89i1-S.7008
29. Nonomura Y, Yasumoto M, Yoshimura R, et al. Relationship between bone marrow cellularity and apparent diffusion coefficient. Magn Reson Imag. 2001;13:757–60. https://doi.org/10.1002/jmri.1105.

30. Messiou C, Kaiser M. Whole body diffusion weighted MRI – a new view of myeloma. Br J Haematol. 2015;171:29–37. https://doi.org/10.1111/bjh.13509.
31. Jacobs MA, Pan L, Macura KJ. Whole-body diffusion-weighted and proton imaging: a review of this emerging technology for monitoring metastatic cancer. Semin Roentgenol. 2009;44:111–22. https://doi.org/10.1053/j.ro.2009.01.003.
32. Belotti A, Ribolla R, Cancelli V, et al. Predictive role of diffusion-weighted whole-body MRI (DW-MRI) imaging response according to MY-RADS criteria after autologous stem cell transplantation in patients with multiple myeloma and combined evaluation with MRD assessment by flow cytometry. Cancer Med. 2021;10:5859–65. https://doi.org/10.1002/cam4.4136.
33. Paternain A, García-Velloso MJ, Rosales JJ, et al. The utility of ADC value in diffusion-weighted whole-body MRI in the follow-up of patients with multiple myeloma. Correlation study with 18F-FDG PET-CT. Eur J Radiol. 2020;133:109403. https://doi.org/10.1016/j.ejrad.2020.109403.
34. Messiou C, Giles S, Collins DJ, et al. Assessing response of myeloma bone disease with diffusion-weighted MRI. BJR. 2012;85:e1198–203. https://doi.org/10.1259/bjr/52759767.
35. Dong H, Huang W, Ji X, et al. Prediction of early treatment response in multiple myeloma using MY-RADS total burden score, ADC, and fat fraction from whole-body MRI: impact of anemia on predictive performance. Am J Roentgenol. 2022;218:310–9. https://doi.org/10.2214/AJR.21.26534.
36. Bray TJP, Singh S, Latifoltojar A, et al. Diagnostic utility of whole body Dixon MRI in multiple myeloma: a multi-reader study. PLoS One. 2017;12: e0180562. https://doi.org/10.1371/journal.pone.0180562.
37. Chenevert TL. Diffusion magnetic resonance imaging: an early surrogate marker of therapeutic efficacy in brain tumors. J Natl Cancer Inst. 2000;92:2029–36. https://doi.org/10.1093/jnci/92.24.2029.
38. Alyas F, Saifuddin A, Connell D. MR imaging evaluation of the bone marrow and marrow infiltrative disorders of the lumbar spine. Magn Reson Imag Clin N Am. 2007;15:199–219. https://doi.org/10.1016/j.mric.2007.03.002.
39. Dutoit JC, Verstraete KL. MRI in multiple myeloma: a pictorial review of diagnostic and post-treatment findings. Insights Imag. 2016;7:553–69. https://doi.org/10.1007/s13244-016-0492-7.
40. Hameed M, Sandhu A, Soneji N, et al. Pictorial review of whole body MRI in myeloma: emphasis on diffusion-weighted imaging. BJR. 2020;93:20200312. https://doi.org/10.1259/bjr.20200312.
41. Bladé J, Beksac M, Caers J, et al. Extramedullary disease in multiple myeloma: a systematic literature review. Blood Cancer J. 2022;12:45. https://doi.org/10.1038/s41408-022-00643-3.
42. Batsukh K, Lee S-E, Min GJ, et al. Distinct clinical outcomes between paramedullary and extramedullary lesions in newly diagnosed multiple myeloma. Immune Netw. 2017;17:250. https://doi.org/10.4110/in.2017.17.4.250.
43. Rosiñol L, Beksac M, Zamagni E, et al. Expert review on soft-tissue plasmacytomas in multiple myeloma: definition, disease assessment and treatment considerations. Br J Haematol. 2021;194:496–507. https://doi.org/10.1111/bjh.17338.
44. Ruiz Santiago F, Láinez Ramos-Bossini AJ, Wáng YXJ, et al. The value of magnetic resonance imaging and computed tomography in the study of spinal disorders. Quant Imag Med Surg 2022;12:3947–3986. https://doi.org/10.21037/qims-2022-04
45. Baudrez V, Galant C, Vande Berg BC. Benign vertebral hemangioma: MR-histological correlation. Skeletal Radiol. 2001;30:442–6. https://doi.org/10.1007/s002560100390.
46. Winfield JM, Poillucci G, Blackledge MD, et al. Apparent diffusion coefficient of vertebral haemangiomas allows differentiation from malignant focal deposits in whole-body diffusion-weighted MRI. Eur Radiol. 2018;28:1687–91. https://doi.org/10.1007/s00330-017-5079-2.
47. Chiabai O, Van Nieuwenhove S, Vekemans M-C, et al. Whole-body MRI in oncology: can a single anatomic T2 Dixon sequence replace the combination of T1 and STIR sequences to detect skeletal metastasis and myeloma? Eur Radiol. 2022;33:244–57. https://doi.org/10.1007/s00330-022-09007-8.
48. Hu HH, Börnert P, Hernando D, et al. ISMRM workshop on fat–water separation: Insights, applications and progress in MRI. Magn Reson Med. 2012;68:378–88. https://doi.org/10.1002/mrm.24369.
49. Koutoulidis V, Terpos E, Papanikolaou N, et al. Comparison of MRI features of fat fraction and ADC for early treatment response assessment in participants with multiple myeloma. Radiology. 2022;304:137–44. https://doi.org/10.1148/radiol.211388.